Energetic ion spectral characteristics in the Saturnian magnetosphere using Cassini/MIMI measurements

K. Dialynas,[1,2] S. M. Krimigis,[1,3] D. G. Mitchell,[3] D. C. Hamilton,[4] N. Krupp,[5] and P. C. Brandt[3]

Received 18 September 2008; revised 5 November 2008; accepted 18 November 2008; published 29 January 2009.

[1] We report sample results on Saturn magnetospheric energetic ion spectral shapes using measurements obtained from the Magnetospheric Imaging Instrument (MIMI) suite onboard Cassini. The ion intensities are measured by the Charge Energy Mass Spectrometer (CHEMS) that covers the energy range of 3 to 236 keV/e, the Low Energy Magnetospheric Measurements System (LEMMS) covering the energy range of $0.024 < E < 18$ MeV, and the Ion Neutral Camera (INCA) that provides ion measurements in the ion mode at the energy range ~5.5 to >220 keV for protons. The data used cover several passes from the period 1 July 2004 to 10 April 2007, at various latitudes over the dipole L range $5 < L < 20$ R_S. The spectra generally show a power law in energy form at larger L values but display a flattening/relative peak at lower ($L < 10$) values centered at ~50 to ~100 keV and can be fit by a κ distribution function with characteristic kT ranging from ~10 to ~100 keV. The results are consistent with the assumption that energetic protons are heated adiabatically as they move inward to stronger magnetic fields, in contrast to the singly ionized oxygen that seems to be heated locally at each L shell. The lack of any trend of the O^+ temperature versus L shell implies that nonadiabatic energization mechanisms and charge exchange with Saturn's neutral gas cloud play an important role for ion energetics.

Citation: Dialynas, K., S. M. Krimigis, D. G. Mitchell, D. C. Hamilton, N. Krupp, and P. C. Brandt (2009), Energetic ion spectral characteristics in the Saturnian magnetosphere using Cassini/MIMI measurements, *J. Geophys. Res.*, *114*, A01212, doi:10.1029/2008JA013761.

1. Introduction

[2] Energetic charged particles in the magnetospheric environment of Saturn were first studied by Pioneer 11 [*Van Allen et al.*, 1980; *Fillius et al.*, 1980] and subsequently by the Low Energy Charged Particle (LECP) instrument on board Voyager 1 and Voyager 2 spacecraft [*Krimigis et al.*, 1981, 1982, 1983]. The Voyagers encounters at Saturn revealed a complex and dynamic magnetosphere and a plasma population of varying elemental composition [*Hamilton et al.*, 1983], with the ring system and the icy satellites modulating the planetary plasma environment [*Carbary et al.*, 1983]. These findings were corroborated and studied in greater detail 24 years later by the MIMI instrument on board the Cassini spacecraft [*Krimigis et al.*, 2005; *Krupp et al.*, 2005]. The icy Saturnian satellites do not significantly affect keV ions in terms of intensities, in contrast to more energetic ions and electrons [*Roussos et al.*, 2007]. In addition, the region of the inner to middle magnetosphere was found to be highly variable and could well be dominated by a series of injections [*Mauk et al.*, 2005], like the cases of Earth and Jupiter.

[3] These observations showed that within the inner magnetosphere of Saturn an extensive neutral cloud exists that contributes strongly to the modulation of the plasma environment. *Sittler et al.* [2008], using Cassini Plasma Spectrometer (CAPS) observations and a neutral model by *Johnson et al.* [2006], provided calculations of the neutral production rates and ion flux tube content within the inner magnetosphere, showing that Enceladus plumes could be a dominant source of neutrals. *Rymer et al.* [2007], by performing phase space density analyses of the electron measurements, confirmed that cool electrons (<100 eV) have a source within the inner magnetosphere and that those electrons are likely products of ionization processes in Saturn's neutral cloud.

[4] A necessary step toward understanding these processes is a full characterization of the energetic particle distributions. Energetic ion composition analyses are critical to establishing their sources and understanding the way they are accelerated within the Saturnian magnetosphere. The

[1]Office for Space Research and Applications, Academy of Athens, Athens, Greece.
[2]Department of Astrophysics, Astronomy and Mechanics, Faculty of Physics, National Kapodistrian University of Athens, Athens, Greece.
[3]Johns Hopkins University Applied Physics Laboratory, Laurel, Maryland, USA.
[4]Department of Physics, University of Maryland, College Park, Maryland, USA.
[5]Max-Planck-Institut für Sonnensystemforschung, Katlenburg-Lindau, Germany.

0148-0227/09/2008JA013761

Table 1. List of Instrument Characteristics Considered in This Study[a]

	LEMMS	CHEMS	INCA
Energy range	0.024 to 18 MeV	3 to 236 keV/e	~3 keV to >220 keV, for H 32 keV to >844 keV for O
Angular resolution	15° cone swept through a plane, segmented by 22.5° per subsector (16 subsectors)	three independent telescopes with 53°FOV each × 4°	~8° × 4°, E_H >50 keV >8° × 8°, E_H ~20 keV
Time resolution	86 s per rotation[b] 5.31 s per subsector 0.66 s per microsector	minimum TOF: 6 ns maximum TOF: 523 ns 0.511 ns per channel	6 s, PHA events 85 s, low resolution 6 min, high resolution 23 min, full sky

[a]In some cases values in this table differ slightly from those published by *Krimigis et al.* [2004].
[b]Since day 33/2005 (2 February 2005), due to technical problem, the LEMMS instrument was locked at ~77° with respect to the spacecraft *z* axis.

principal results of this study show that energetic protons exhibit different behavior from singly ionized oxygen as they are transported into stronger magnetic fields closer to the planet. Generally, H^+ particles appear to be heated adiabatically with decreasing *L* shell while O^+ particles appear to be heated locally. The energetic ion spectral evolution with decreasing *L* shell shows that Saturn's neutral cloud plays a key role in the ion-neutral gas interactions in the magnetosphere of Saturn, presenting a significant loss term of the ~30 to 100 keV ions via the charge exchange process.

2. Experiment and Data Analysis Details

[5] The MIMI experiment on board Cassini consists of CHEMS that measures ion species and their charge state, LEMMS that separately measures ion and electron intensities in different energy ranges, and an Ion Neutral Camera (INCA) designed to separately detect energetic ions or energetic neutral atoms (ENAs), depending on sensor mode [*Krimigis et al.*, 2004]. The instruments characteristics are described in detail by *Krimigis et al.* [2004] and briefly at Table 1. In the present study, we employed ion intensity data using all three MIMI sensors for days 183/2004 to 100/2007 and for dipole *L* values between $L = 5\ R_S$ and $L = 20\ R_S$. During the period 265/2005 to 182/2006 the Cassini spacecraft surveyed Saturn's magnetosphere very close to the nominal magnetic equatorial plane, while orbits during late 2006 to 2007 sampled higher latitudes up to ~50 degrees.

[6] To produce the proton spectra, we utilized LEMMS A_0-A_7 energy channels (assumed to be mostly dominated by protons) that cover the energy range of 30.7 keV to 2.3 MeV and INCA time of flight (TOF) energy channels which occupy the 5.5 keV to 338 keV energy range. The Oxygen ion spectra were obtained using CHEMS 9 keV/e to 226 keV/e for O^+ and water products and combined them with INCA 39 keV to 677 keV O^+ energy channels measurements.

[7] High-energy cosmic rays penetrate the Saturnian magnetosphere, contribute to the counting rate of the LEMMS sensor detectors, and can lead to overestimates of the ion fluxes measured by LEMMS in low-intensity regions. In order to subtract the cosmic ray background within the Kronian magnetosphere, we followed cosmic ray intensity changes from 2004 to 2007 by using two different periods during quiet times for LEMMS measurements. Specifically, we surveyed the time periods from the SOI to late 2007 and identified those days that the Cassini spacecraft was outside the Saturnian magnetopause detecting the lowest intensities. Sampled measurements on days 286/2004 and 208/2007 were used as background values for the time periods 2004–2005 and 2006–2007, respectively. During both cases, LEMMS's high-energy electron channels (*E* channels) did not present any fluctuations. We also note that we carefully excluded periods with solar energetic particle activity. Nevertheless, some residual background effects are still seen during very low intensity periods, but those signatures are easily recognized and have been extracted from the analysis.

3. Proton and Oxygen Ion Spectra

[8] Figure 1 illustrates sampled 30 min accumulation time H^+ (top) and O^+ spectra (bottom) within the magnetospheric regions of $5 < L < 20\ R_S$. The triangles and squares are the measured ion INCA and LEMMS (for H^+) and CHEMS (for O^+) data, respectively, while the lines are the fits determined in a least square sense using a Levenberg-Marquardt method [*Levenberg*, 1944; *Marquardt*, 1963] which is one of the most widely used optimization methods in solving nonlinear curve fitting problems. It interpolates between the method of gradient descent and the Gauss-Newton algorithm while being more robust than Gauss-Newton method since it gives the opportunity of finding the optimum solution even if it starts relatively far from the minimum. The subtitles of the spectra plots contain the spatial information and the fit parameters which are optimized to minimize the least squares differences between the measured and calculated fluxes.

[9] As is evident from the sample spectra in Figure 1, the H^+ have higher intensities for the magnetospheric regions shown, whereas the O^+ intensities for the ~30–200 keV energy range become comparable to protons closer to the planet. The shape of the spectrum evolves with decreasing *L* shell revealing the formation of a spectral flattening for $L < 15\ R_S$ that occurs in the 30–150 keV energy range for both H^+ and O^+, which becomes even more prominent in the magnetospheric regions <10 R_S. The ~30–100 keV energy range decrease in the intensities seen in Figure 1 for both H^+ and O^+ in the innermost regions of the Saturnian magnetosphere <10 R_S [cf. *Mauk et al.*, 2005], where part of the neutral cloud is confined [*Esposito et al.*, 2005], is a result of ion-neutral gas interaction losses.

[10] *Young et al.* [2005] showed broad peaks in counting rates of cold ions at low energies, at local corotation speeds. Therefore, the turn-up in the intensities seen in Figure 1 for

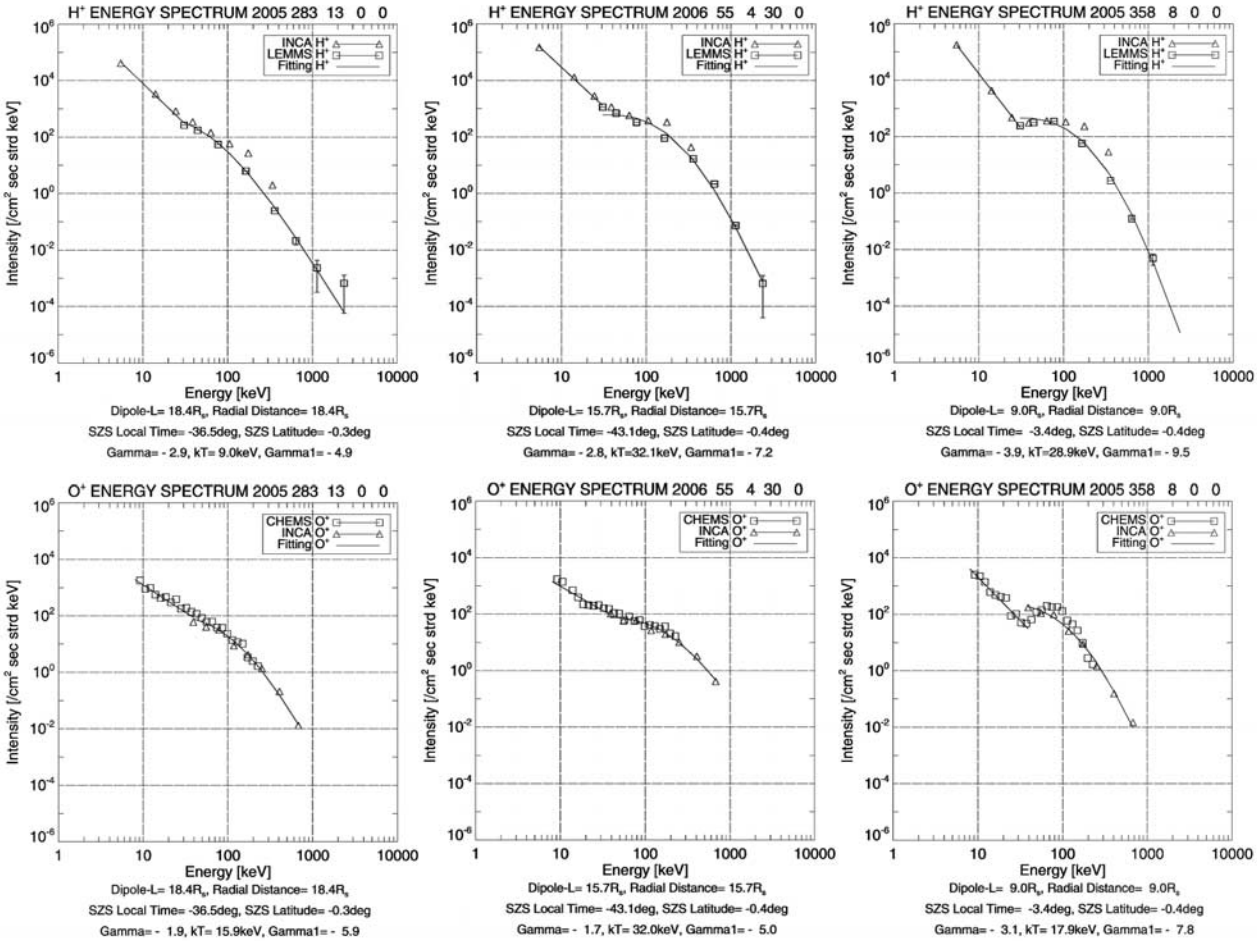

Figure 1. (top) Sampled proton spectra using combined INCA and LEMMS data in the energy range of 5.5 to 2300 keV and (bottom) oxygen ion spectra using combined CHEMS-INCA data in the energy range 9 to 677 keV over selected magnetospheric regions and the corresponding fittings. Measured intensity error bar amplitudes are comparable or smaller than the data points on the diagrams, unless otherwise noted.

<30 keV ions is possibly the high-energy tail of that cold ion population. As expected, ions continue charge exchanging with neutrals in the 5 to 30 keV energy range and that is maybe the reason for the observed change in slope on this part of the distribution. When a $\sim$5–100 keV ion interacts with the neutrals a new cold ion is created at corotation speeds which consequently populates the low-energy plasma distribution. Assuming that those newborn ions do not undergo further charge exchange collisions, they are adiabatically accelerated, by conserving the first adiabatic invariant, moving inward to higher energies than the local corotation energies. For the H^+, this change in slope, the slight increase of the spectral index seen in Figure 1 for the 5.5 to 30 keV energy range with decreasing L shell is statistically significant, in contrast to the O^+ where the slope of the spectra in the 9 to 39 keV energy range does not show a specific trend with L value.

[11] The spectral shape used in this study is a combination of a power law for the low-energy range and an equivalent to the κ distribution function defined originally by *Vasyliunas* [1968] for the middle- and high-energy range of the energetic ion spectra. Although κ distribution function is usually expressed in terms of phase space density, we will henceforth use κ distribution function in terms of differential intensities. The mathematical expression of Vasyliunas κ distribution function is

$$j[E] = \frac{Nw_0}{E_0} \frac{2\pi \cdot \Gamma(\kappa+1)}{(\pi\kappa)^{3/2}\Gamma(\kappa-1/2)} \frac{E/E_0}{(1+E/\kappa \cdot E_0)^{\kappa+1}} \quad (1)$$

where $j[E]$ is the differential particle flux per unit energy, N is the total number density, w_0 is the most probable speed, E_0 is the corresponding energy (i.e., 1/2 mw_0^2) and κ is the exponent of the differential flux at high energies. *Mauk et al.* [2004] introduced a modified Kappa distribution function to characterize the energetic ion spectra sampled within the Jovian magnetosphere using ion measurements obtained by the Energetic Particle Detector (EPD) experiment on board Galileo spacecraft:

$$j = C \cdot \frac{E \cdot [E_1 + kT(1+\gamma_1)]^{-1-\gamma_1}}{1+(E_1/et)^{\gamma_2}} \quad (2)$$

where j is the differential intensity, E is the measured energy, E_1 is energy as measured with respect to the frame of reference moving with the plasma flow (e.g., $E = E_1$, if all measurements are made in the frame of reference moving with the plasma flow). The numerator of equation (2) is equivalent to the κ distribution function as expressed by equation (1) with kT being the ion temperature and γ_1 being the high-energy spectral index. The denominator of equation (2) is an additional term to characterize any softening break in slope (γ_2) at very high energies with the transition energy given roughly by the parameter et.

[12] The spectral shape in the present case clearly implies that the MIMI instruments may be detecting the high-energy tail of a κ distribution function that maybe centered at ion temperatures ~1 keV or lower and a second kappa function which is visible in our data set. Specifically, the 5.5–30.7 keV combined INCA-LEMMS H^+ and 9–39 keV combined CHEMS-INCA O^+ data were fitted using a simple power law:

$$j = C \cdot E^{-\gamma} \tag{3}$$

while the 30.7–2300 KeV combined INCA-LEMMS H^+ and 39–677 keV combined CHEMS-INCA O^+ data were fitted using a Kappa distribution function:

$$j = C \cdot E[E + kT(1 + \gamma_1)]^{-(1+\gamma_1)} \tag{4}$$

as used by *Paranicas et al.* [1999] and *Mauk et al.* [2004], slightly modified since there are no observed softening breaks in the high-energy tail in our data. In this case, j is the measured particle differential intensity expressed in counts/(cm^2 s sr keV), E is the measured energy (detector energy channels) expressed in keV, γ and γ_1 represent the power law spectral index and the spectral index referring to the κ distribution's function high-energy tail, respectively, while kT is the particle (H^+ and O^+ in our case) temperature for the kappa portion of the distribution expressed in keV. In this paper, when we use the word "temperature" we refer to a type of partial temperature corresponding to the suprathermal plasma population at Saturn. We have treated the spectral indices (γ and γ_1), as well as the temperature (kT), as free fitting parameters using 30 min averaged data. We note that the 30 min averaging was selected mostly to insure good statistics for the measurements, while assuring that spatial effects are minimized during such accumulation.

[13] Figure 2 (top left) shows the proton temperature profile with increasing L shell as derived from the fittings described earlier in this study. *Krimigis et al.* [1983] using a very limited set of Voyager 1 and Voyager 2 data estimated proton temperature profiles by fitting the ion intensities measured with the LECP energy channels. The results presented in the present study are generally in good agreement with the equivalent *Krimigis et al.* [1983] results, although the calculated temperatures below 10 R_S seem to be significantly higher here (by a factor of ~1.5 in some cases) than those presented in the aforementioned Voyagers paper. The LECP data showed a substantial difference in the proton temperature profile between the Voyager 1 and Voyager 2 encounters, as well as variability with time scales of about a day between the inbound and outbound trajectories. The Cassini spacecraft provides a much denser spectral information than the Voyagers.

[14] The blue line included in Figure 2 is a power law fit at L values (a reference line) that describes the observed trend in the proton temperatures as a function of L shell, showing that in fact the protons seem to be adiabatically accelerated while moving toward stronger magnetic fields closer to the planet. Outside ~13 R_S the temperature profile appears quite variable and the dipole approximation breaks so that this line fails to fit the temperature data. Adiabatic heating to energies greater than 100 eV occurs also in the case of inward moving electrons as shown by *Rymer et al.* [2008]. Figure 2 (bottom left) represents the derived spectral index (γ_1) as a function of L shell for the H^+ particles in the 30 keV to 3.7 MeV energy range. The observed trend in this case is for the spectral index to increase with decreasing L shell. By analogy with the case of proton temperatures, the diagram appears quite scattered, with the spectral indices varying from ~2.5 to 12.5 throughout the whole region of $5 < L < 20$ R_S.

[15] By contrast, the O^+ temperature (Figure 2, top right) does not seem to present any significant trend with decreasing L value. The same applies for the O^+ spectral index as a function of L shell (Figure 2, bottom right). Both the 39 to 677 keV energy range O^+ temperatures and spectral indices remain almost flat with L shell. As in the case of H^+, the O^+ temperature and spectral index profiles are highly variable. The temperature and spectral index distributions that refer to equatorial and non equatorial passes (red and black points, respectively) for both H^+ and O^+ show that there appears to be no latitude dependence. The hard lower boundary which can be seen at Figure 2 at the calculated gammas for protons in the outer magnetosphere and for oxygen for all L shells could probably be attributed to either instrument or averaging effects.

[16] In order to test the aforementioned results we have calculated the characteristic energy (E_C) profiles for both species (not shown here) by taking the ratio of the integral energy intensity (I_E) and the integral number intensity (I_n) [e.g., *Mauk et al.*, 2004] and this result is consistent with the temperature profiles shown in this paper.

4. Summary and Discussion

[17] By combining particle intensity measurements among the MIMI instruments onboard Cassini, we were able to model the energetic ion spectra throughout the magnetosphere of Saturn for L values from 5 to 20 R_S. The ~30 to 150 keV energy range clearly shows the formation of a peak in the spectra for both H^+ and O^+ below ~15 R_S that evolves with decreasing L shell becoming more prominent in the region below ~10 R_S. This region involves complex dynamics since this is where part of the ring current exists as identified by *Sergis et al.* [2007] using Cassini/MIMI particle data and earlier by *Connerney et al.* [1983] using magnetic field observations along with *Krimigis et al.* [1983] and *Mauk et al.* [1985] using energetic particle data from Voyagers 1 and 2. ENA observations [*Paranicas et al.*, 2005; *Mitchell et al.*, 2005a] suggest that charge-exchange interactions take place between the energetic ions and the neutrals in this region, a fact that explains the decrease in ion intensities observed in

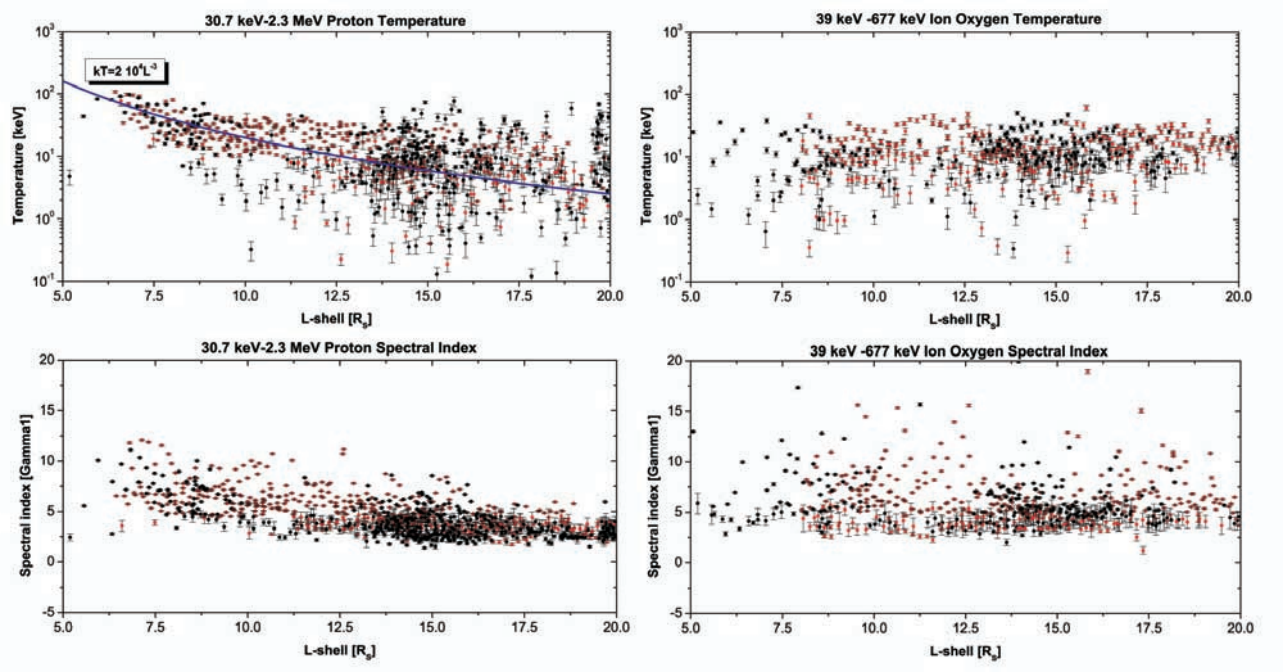

Figure 2. (top left) Proton temperature profile (in keV) as a function of L shell ($5 < L < 20$ R_S). The temperatures are calculated from direct fittings with a kappa distribution function in the energy range of 30.7–2300 keV. The blue line is a power law fit at L values (a reference line) that describes the observed trend in the proton temperatures with L shell. The temperature profile shows that protons are accelerated adiabatically with decreasing L shell. (bottom left) H^+ spectral index (γ_1) as a function of L shell ($5 < L < 20$ R_S). The gammas are calculated from direct fits with the kappa distribution function described in the text in the energy range of 30.7–2300 keV. (top right) Singly ionized oxygen temperature profile (in keV) and (bottom right) spectral index (γ_1) with L shell for magnetospheric regions of $5 < L < 20$ R_S. The ion oxygen temperatures and spectral indices are derived using a kappa distribution function in the energy range of 39 to 677 keV data. As in the case of protons, the profiles seen in both panels for the oxygen seem highly variable but they do not present any specific trend with L shell. Red points refer to temperatures calculated from spectra sampled in the equatorial plane.

the spectra for energies below ~100 keV [*Paranicas et al.*, 2008]. In addition, the evolving peak can be attributed to energization processes similar to the ones found at Earth [e.g., *Kistler et al.*, 1989].

[18] We provided analytical fits to ion intensities using a combination of a power law for the low-energy range of the MIMI data and an equivalent to the κ distribution function for the middle and high energy range. The results show that the proton distributions become more energetic with decreasing L shell as a consequence of the increasing magnetic field and conservation of the first adiabatic invariant ($\mu = W_\perp/B$, where $W_\perp$ is the perpendicular energy and B is the magnetic field magnitude) related to the motion of a particle within the Kronian magnetic field.

[19] In contrast, the singly ionized oxygen seems to be heated locally at each L shell. As explained in the previous paragraph, we know that adiabatic heating should take place for all particles, so this means that little energy is gained by adiabatic heating as O^+ ions move toward the planet (if they do) to stronger magnetic fields. The O^+ lifetime within the inner to middle magnetosphere (<10 R_S) is much shorter than the H^+ lifetime in the same region due to charge-exchange interactions of these ions with the neutral cloud particles. In Figure 3 it is clear that O^+ and H^+ lifetimes become equal at ~20 keV, while for energies greater than 20 keV the O^+ particles begin to have much shorter lifetimes than H^+ with increasing energy (e.g., by a factor of 4 at ~100 keV). Although O^+ particles travel slower by a factor of 4 compared to H^+ particles with the same kinetic energies, the charge-exchange cross sections [cf. *McEntire and Mitchell*, 1989] in the ~30 to 150 keV energy range where the plateau and the decrease in the intensities occurs for O^+ impacting either neutral O or H are significantly higher than the cross sections related to H^+ interactions with the neutral O and H in the same energy range.

[20] As shown by *Jurac and Richardson* [2005], the H_2O is the dominant neutral near satellite sources (with peak densities over 1000/cm^3 from Enceladus to Mimas) while OH is dominant elsewhere (with peak densities over 1000/cm^3 near Enceladus and 600/cm^3 near Mimas). Although Figure 3 displays the O^+ and H^+ lifetimes due to charge exchange collisions with the neutral O cloud, we should note that the ion lifetimes would be considerably smaller within the inner magnetosphere (of the order of a few hours) if the OH and H_2O densities are taken into consideration along with the equivalent H and O. Owing to their smaller charge-exchange cross sections the H^+ particles can survive much more efficiently at all distances, throughout the whole region where the neutral cloud is confined than the O^+.

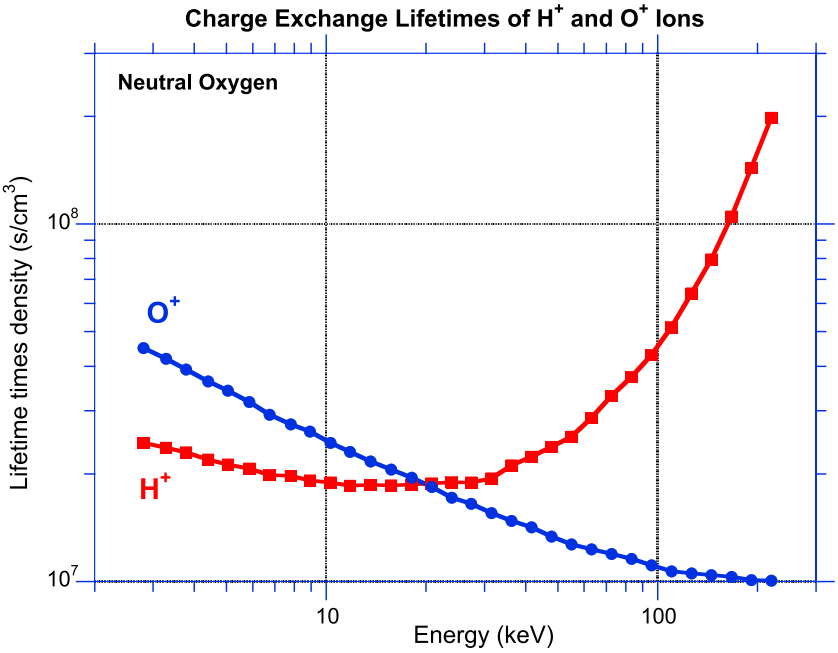

Figure 3. Estimated H^+ and O^+ lifetimes multiplied with neutral density due to charge exchange with neutral oxygen for the energy range of ~3 to 200 keV. Ion lifetimes are estimated using the equation t (sec) = 1/(v σ n), where v is each particle's velocity in cm/s, σ the charge exchange cross section in cm^2 and n is the neutral density in $/cm^3$ (O density in this case).

[21] By using a typical O^+ spectrum at ~16 R_S and progressively projecting it to ~5 R_S we were able to simulate the charge exchange effect postulated above from our analysis on the O^+ temperatures (not shown here). It is noted that the opposite effect was inferred by *Mauk et al.* [2004] but their analysis focused on the ≫100 keV part of the ion distribution in the Jovian magnetosphere. Future work will examine the details of this process, taking into account both, the ion spectra observed in situ, the ENA spectra together with the local density profile of neutral H and O to attain a self-consistent picture for the complete process.

[22] The question that emerges from our results is how the O^+ particles are energized locally at each *L* shell and why the H^+ particles are not subjected to the same energization mechanism. This characteristic is not inconsistent with acceleration in rapid magnetic field reconfigurations where the gyroperiod of O^+ is too long compared to that of protons to conserve the first adiabatic invariant. Dramatic non-adiabatic acceleration of O^+ (and not protons) have been observed and explained in Earth's magnetosphere [*Fok et al.*, 2006; *Delcourt*, 2002]. Recent studies by *Mitchell et al.* [2005b] and [*Carbary et al.*, 2008] have shown that protons and O^+ have different behaviors that are consistent with the expected non-adiabatic behavior of O^+ during rapid magnetic field reconfigurations in the region between 15 and 40 R_S.

[23] **Acknowledgments.** We thank M. Kusterer and J. Vandegriff (Johns Hopkins University Applied Physics Laboratory) for assistance with the data reduction. We are grateful to B. H. Mauk and C. P. Paranicas as well as all colleagues on the MIMI team, who provided valuable comments that have improved the presentation. Work at JHUAPL was supported by NASA under contract NAS5–97271 and NNX07AJ69G and by subcontracts at the University of Maryland and the Office for Space Research and Applications of the Academy of Athens. The German contribution of MIMI/LEMMS was financed in part by the Bundesministerium für Bildung und Forschung (BMBF) through the Deutsches Zentrum für Luft-und Raumfahrt e.V. (DLR) and by the Max-Planck-Gesellschaft.

[24] Wolfgang Baumjohann thanks Thomas Armstrong and another reviewer for their assistance in evaluating this paper.

References

Carbary, J. F., S. M. Krimigis, and W. H. Ip (1983), Energetic particle microsignatures of Saturn's satellites, *J. Geophys. Res.*, *88*, 8947–8958, doi:10.1029/JA088iA11p08947.

Carbary, J. F., D. G. Mitchell, P. Brandt, C. Paranicas, and S. M. Krimigis (2008), ENA periodicities at Saturn, *Geophys. Res. Lett.*, *35*, L07102, doi:10.1029/2008GL033230.

Connerney, J. E. P., M. H. Acuña, and N. F. Ness (1983), Currents in Saturn's magnetosphere, *J. Geophys. Res.*, *88*, 8779–8789, doi:10.1029/JA088iA11p08779.

Delcourt, D. C. (2002), Particle acceleration by inductive electric fields in the inner magnetosphere, *J. Atmos. Sol. Terr. Phys.*, *64*, 551–559, doi:10.1016/S1364-6826(02)00012-3.

Esposito, W. L., et al. (2005), Ultraviolet imaging spectroscopy shows an active Saturnian system, *Science*, *307*, 1251–1255, doi:10.1126/science.1105606.

Fillius, W., W. H. Ip, and C. E. McIlwain (1980), Trapped radiation belts of Saturn: First look, *Science*, *207*, doi:10.1126/science.207.4429.425.

Fok, M.-C., T. E. Moore, P. C. Brandt, D. C. Delcourt, S. P. Slinker, and J. A. Fedder (2006), Impulsive enhancements of oxygen ions during substorms, *J. Geophys. Res.*, *111*, A10222, doi:10.1029/2006JA011839.

Hamilton, D. C., G. Gloeckler, S. M. Krimigis, and W. I. Axford (1983), Energetic atomic and molecular ions in Saturn's Magnetosphere, *J. Geophys. Res.*, *88*, 8905–8922, doi:10.1029/JA088iA11p08905.

Johnson, R. E., H. T. Smith, O. J. Tucker, M. Liu, M. H. Burger, E. C. Sittler Jr., and R. L. Tokar (2006), The Enceladus and OH tori at Saturn, *Astrophys. J.*, *644*, L137–L139, doi:10.1086/505750.

Jurac, S., and J. D. Richardson (2005), A self consistent model of plasma and neutrals at Saturn: Neutral cloud mosrphology, *J. Geophys. Res.*, *110*, A09220, doi:10.1029/2004JA010635.

Kistler, L. M., F. M. Ipavich, D. C. Hamilton, and G. Gloeckler (1989), Energy spectra of the major ion species in the ring current during geomagnetic storms, *J. Geophys. Res.*, *94*, 3579–3599, doi:10.1029/JA094iA04p03579.

Krimigis, S. M., T. P. Armstrong, W. I. Axford, C. O. Bostrom, G. Gloekler, E. P. Keath, L. J. Lanzerotti, J. F. Carbary, D. C. Hamilton, and E. C.

Roelof (1981), Low-energy charged particles in Saturn's magnetosphere-Results from Voyager 1, *Science*, *212*, 225–231, doi:10.1126/science.212.4491.225.

Krimigis, S. M., T. P. Armstrong, W. I. Axford, C. O. Bostrom, G. Gloeckler, E. P. Keath, L. J. Lanzerotti, J. F. Carbary, D. G. Hamilton, and E. C. Roelof (1982), Low-energy hot plasma and particles in Saturn's magnetosphere, *Science*, *215*, 571–577, doi:10.1126/science.215.4532.571.

Krimigis, S. M., J. F. Carbary, E. P. Keath, T. P. Armstrong, L. J. Lanzerotti, and G. Gloeckler (1983), General characteristics of hot plasma and energetic particles in the Saturnian magnetosphere-Results from the Voyager spacecraft, *J. Geophys. Res.*, *88*, 8871–8892, doi:10.1029/JA088iA11p08871.

Krimigis, S. M., et al. (2004), Magnetosphere Imaging Instrument (MIMI) on the Cassini Mission to Saturn/Titan, *Space Sci. Rev.*, *114*, 233–329, doi:10.1007/s11214-004-1410-8.

Krimigis, S. M., et al. (2005), Dynamics of Saturn's magnetosphere from MIMI during Cassini's orbital insertion, *Science*, *307*, 1270–1273, doi:10.1126/science.1105978.

Krupp, N., et al. (2005), The Saturnian plasma sheet as revealed by energetic particle measurements, *Geophys. Res. Lett.*, *32*, L20S03, doi:10.1029/2005GL022829.

Levenberg, K. (1944), A method for the solution of certain problems in least squares, *Q. Appl. Math.*, *2*, 164–168.

Marquardt, D. (1963), An algorithm for least squares estimation on nonlinear parameters, *SIAM J. Appl. Math.*, *11*, 431–441, doi:10.1137/0111030.

Mauk, B. H., S. M. Krimigis, and R. P. Lepping (1985), Particle and field stress balance within a planetary magnetosphere, *J. Geophys. Res.*, *90*, 8253–8264, doi:10.1029/JA090iA09p08253.

Mauk, B. H., D. G. Mitchell, R. W. McEntire, C. P. Paranicas, E. C. Roelof, D. J. Williams, and S. M. Krimigis (2004), Energetic ion characteristics and neutral gas interactions in Jupiter's magnetosphere, *J. Geophys. Res.*, *109*, A09S12, doi:10.1029/2003JA010270.

Mauk, B. H., et al. (2005), Energetic particle injections in Saturn's magnetosphere, *Geophys. Res. Lett.*, *32*, L14S05, doi:10.1029/2005GL022485.

McEntire, R. W., and D. G. Mitchell (1989), Instrumentation for global magnetospheric imaging via energetic neutral atoms, in *Solar System Plasma Physics, Geophys. Monogr. Ser.*, vol. 54, edited by J. H. Waite Jr., J. L. Burch, and R. L. Moore, pp. 69–80, AGU, Washington, D.C.

Mitchell, D. G., P. C. Brandt, E. C. Roelof, J. Dandouras, S. M. Krimigis, and B. H. Mauk (2005a), Energetic neutral atom emissions from Titan interaction with Saturn's magnetosphere, *Science*, *308*, 989–992, doi:10.1126/science.1109805.

Mitchell, D. G., et al. (2005b), Energetic ion acceleration in Saturn's magetosphere: Substorms on Saturn?, *Geophys. Res. Lett.*, *32*, L20S01, doi:10.1029/2005GL022647.

Paranicas, C., W. R. Paterson, A. F. Cheng, B. H. Mauk, R. W. McEntire, L. A. Frank, and D. J. Williams (1999), Energetic particle observations near Ganymede, *J. Geophys. Res.*, *104*, 17,459–17,467, doi:10.1029/1999JA900199.

Paranicas, C., D. G. Mitchell, E. C. Roelof, P. C. Brandt, D. J. Williams, S. M. Krimigis, and B. H. Mauk (2005), Periodic intensity variations in global ENA images of Saturn, *Geophys. Res. Lett.*, *32*, L21101, doi:10.1029/2005GL023656.

Paranicas, C., D. G. Mitchell, S. M. Krimigis, D. C. Hamilton, E. Roussos, N. Krupp, G. H. Jones, R. E. Johnson, J. F. Cooper, and T. P. Armstrong (2008), Sources and losses of energetic protons in Saturn's magnetosphere, *Icarus*, *197*, 519–525, doi:10.1016/j.icarus.2008.05.011.

Roussos, E., G. H. Jones, N. Krupp, C. Paranicas, D. G. Mitchell, A. Lagg, J. Woch, U. Motschmann, S. M. Krimigis, and M. K. Dougherty (2007), Electron microdiffusion in the Saturnian radiation belts: Cassini MIMI/LEMMS observations of energetic electron absorption by the icy moons, *J. Geophys. Res.*, *112*, A06214, doi:10.1029/2006JA012027.

Rymer, A. M., et al. (2007), Electron sources in Saturn's magnetosphere, *J. Geophys. Res.*, *112*, A02201, doi:10.1029/2006JA012017.

Rymer, A. M., B. H. Mauk, T. W. Hill, C. Paranicas, D. G. Mitchell, A. J. Coates, and D. T. Young (2008), Electron circulation in Saturn's magnetosphere, *J. Geophys. Res.*, *113*, A01201, doi:10.1029/2007JA012589.

Sergis, N., S. M. Krimigis, D. G. Mitchell, D. C. Hamilton, N. Krupp, B. M. Mauk, E. C. Roelof, and M. Dougherty (2007), Ring current at Saturn: Energetic particle pressure in Saturn's equatorial magnetosphere measured with Cassini/MIMI, *Geophys. Res. Lett.*, *34*, L09102, doi:10.1029/2006GL029223.

Sittler, E. C., et al. (2008), Ion and neutral sources and sinks within Saturn's inner magnetosphere: Cassini results, *Planet. Space Sci.*, *56*, 3–18, doi:10.1016/j.pss.2007.06.006.

Van Allen, J. A., M. F. Thomsen, B. A. Randall, R. L. Rairden, and C. L. Grosskreutz (1980), Saturn's magnetosphere, rings and inner satellites, *Science*, *207*, 415–421, doi:10.1126/science.207.4429.415.

Vasyliunas, V. M. (1968), A survey of low-energy electrons in the evening sector of the magnetosphere with OGO 1 and OGO 3, *Geophys. Res. Lett.*, *73*, 2839–2884.

Young, D. T., et al. (2005), Composition and dynamics of plasma in Saturn's magnetosphere, *Science*, *307*, 1262–1266, doi:10.1126/science.1106151.

P. C. Brandt and D. G. Mitchell, Johns Hopkins University Applied Physics Laboratory, 11100 Johns Hopkins Road, Laurel, MD 20723, USA.

K. Dialynas and S. M. Krimigis, Office for Space Research and Applications, Academy of Athens, GR-10679 Athens, Greece. (kdialynas@phys.uoa.gr)

D. C. Hamilton, Department of Physics, University of Maryland, College Park, MD 20742, USA.

N. Krupp, Max-Planck-Institut für Sonnensystemforschung, Max-Planck-Strasse 2, D-37191 Katlenburg-Lindau, Germany.